Mechanisms of Ewing sarcoma metastasis : biochemistry and biophysics

Beletkaia, E.

Chapter 2

CXCR4 signaling is controlled by immobilization at the plasma membrane[1]

[1]This chapter is based on: E. Beletkaia, S. F. Fenz, W. Pomp, E. Snaar-Jagalska, P. W. C. Hogendoorn, T. Schmidt, CXCR4 signaling is controlled by immobilization at the plasma membrane (*under review at BBA - Molecular cell research)*

Understanding of the regulation mechanisms of CXCR4 signaling is essential for revealing its role in physiological and pathological processes. Though biochemical pathways following CXCR4 activation by its ligand CXCL12 are well established, knowledge about the receptor dynamics on the plasma membrane remains limited. Here we used Ewing sarcoma-derived cells to unravel the processes that are involved in regulating CXCR4 dynamics on the plasma membrane during receptor signaling. Single-molecule epi-fluorescence microscopy showed that CXCR4 was present in monomeric state on the plasma membrane independent of receptor stimulation. However, upon activation freely diffusing receptors were immobilized in a ligand concentration-dependent manner. CXCR4 immobilization was strongly correlated with the ability for G-protein signaling and was a precursor of subsequent endocytotic events. We found that a balanced regulation of G-protein dependent and independent pathways was required for faithful receptor signal transduction.

2.1 Introduction

Ewing sarcoma is a high-grade aggressive tumor occurring predominantly in bones of young children and adolescent. About a quarter of Ewing sarcoma patients have developed metastasis present at first diagnosis (Kovar, 2014). The characteristic and most common chromosomal translocation fusing a portion of the EWSR1 gene to the FLI gene, t(11;22)(q24;q12), results in the chimeric protein, EWS/FLI. This translocation was shown to change the expression of many different genes (Kovar, 2014). Frequently over-expressed in Ewing sarcoma is the chemokine receptor/ligand CXCR4/CXCL12 axis was suggested to promote tumor progression and cell growth (Berghuis et al. 2012). Additionally, CXCR4 was shown to be associated with Ewing sarcoma metastasis and with a poor prognosis for patients (Kim et al., 2011; Bennani-Baiti et al., 2010). Thus, understanding of the molecular mechanisms of CXCR4 signaling regulation is essential.

The C-X-C chemokine receptor type 4 (CXCR4) belongs to the class of G-protein coupled receptor (GPCRs). CXCR4 selectively binds to the C-X-C chemokine CXCL12. The CXCR4/CXCL12 pathway is biochemically well studied (Teicher and Fricker, 2010). Binding of CXCL12 causes conformational changes of the receptor and promotes activation of the G-protein hetero-trimer. Dissociation of the trimer into G_{α}- and $G_{\beta\gamma}$-subunits leads to initiation of the respective pathways downstream of CXCR4. CXCR4 activates four different G_{α} subunits (Rubin, 2009) with predominant coupling to $G_{\alpha q}$ and $G_{\alpha i}$ (Teicher and Fricker, 2010). Activation of $G_{\alpha q}$ regulates protein kinase C (PKC) signaling that leads to Ca^{2+} release. The $G_{\alpha i}$-pathway involves activation of Akt, Erk1/2 and Cdc42 cascades. Dissociated $G_{\beta\gamma}$ activates phospholipase-C (PLC) and phosphoinositide-3 kinase (PI3K). The ultimate outcome of CXCR4 signaling leads to gene transcription, cell adhesion and cell migration (Busillo and Benovic, 2007; Otsuka and Bebb, 2008; Teicher and Fricker, 2010) and hence can be involved in tumor, e.g. Ewing sarcoma, progression and metastasis.

Frequently GPCR signaling is controlled via receptor dimerization. There is evidence that CXCL12-induced activation of CXCR4 leads to the formation of heterodimers with CCR2 and CXCR7 (Springael et al., 2005; Levoye et al.,2009; Luker et al., 2009; Decaillot et al., 2011). It was shown that CXCR7 can regulate CXCR4-dependent pathways by promoting or inhibiting G-protein activation (Levoye et al.,2009; Decaillot et

al., 2011), or act as a CXCL12 scavenger (Naumann et al., 2010). However, some Ewing sarcoma cells, including cell line A673, do not express CXCR7 nor CCR2 (Bennani-Baiti et al., 2010),thus, heterodimerization of CXCR4 with these receptors is likely unimportant.

Many GPCRs are in a dynamic equilibrium between monomers and homo-dimers on the plasma membrane (Kasai and Kusumi, 2014). BRET experiments imply that a small portion of CXCR4 forms homodimers even in the absence of CXCL12 (Hamatake et al., 2009). Additionally, the CXCR4 crystal structure suggests homodimeric state of CXCR4 (Wu et al., 2010). Some studies report that stimulation with CXCL12 is required for CXCR4 homodimerization (Springael et al., 2005), while others report no dimerization of CXCR4 upon activation (Hamatake et al., 2009).

Alongside with receptor dimerization, internalization of GPCRs is considered a regulatory process. Upon activation CXCR4 promotes β-arrestin recruitment that subsequently leads to receptor internalization. Internalized receptors in turn can be recycled to the plasma membrane or follow the lysosomal path towards breakdown (Busillo and Benovic, 2007). This process is recognized as receptor desensitization. In Ewing sarcoma endocytosis was identified to have a strong impact on receptor signaling (Martins et al., 2011).

Thus, CXCR4 conduct on the plasma membrane is very dynamic and has great impact on the receptor signaling. However, knowledge about CXCR4 dynamics on the plasma membrane is controversial. Hence, we decided to use the high spatial and temporal resolution that is combined in single-molecule microscopy to obtain novel understanding of CXCR4 signaling. In the last decade a number of single-molecule studies were undertaken to study receptor dynamics on the plasma membrane and relate the findings to the signaling outcome (de Keijzer et al., 2008; Ueda et al. 2001; Jacquier et al., 2006; Calebiro et al., 2013; Lill et al., 2005; Ye et al., 2013). Here we investigated the membrane dynamics of CXCR4-eYFP in the Ewing sarcoma derived cell line A673. We observed a correlation between receptor stimulation and mobility. Immobilization of the activated receptor was facilitated via $G_{\alpha i}$ mediated pathway and clathrin-dependent endocytosis. Thus, we found indications that receptor signaling was controlled via a regulatory cross-talk between G-protein dependent and independent pathways.

2.2 Materials and Methods

2.2.1 Cell culture and transfection

A673 cells were maintained in IMDM cell culture medium (Gibco, USA) supplemented with 10% fetal bovine serum (FBS, Gibco, USA) at 37°C and 5% CO_2. To study the CXCR4 receptor, A673 wild type (A673 wt) cells were stably transfected using a retroviral construct encoding for CXCR4-eYFP (kindly provided by Prof. Dr. Nikolaus Heveker, University of Montreal). Viral transfection was performed as follows. 5×10^4 cells/well were seeded in a 24-well plate; the next day, 1 MOI of viral particles and 5 μg/mL polybreen was added for 24 hours, followed by medium refreshment. For experiments A673 cells stably transfected with CXCR4-eYFP (further referred to as A673-CXCR4 cells) were used after three passages.

2.2.2 Sample preparation

For imaging 1x10^5 of A673-CXCR4 cells were placed in 0.35 mm culture dishes (Ibidi, Germany) in 2 mL of complete IMDM medium (with 10% FBS) and left to attach overnight. Before imaging the medium in the samples was replaced with fresh IMDM without serum to minimize autofluorescence. During imaging the CO_2 level was maintained at 5% and temperature at 37°C using the INUBG2E-ZILCS (TokaiHit, Japan).

2.2.3 Global CXCL12 stimulation assay

Activation of the CXCR4 receptor with its specific ligand, CXCL12 (Gibco, USA) was done as global stimulation before imaging: CXCL12 was added to the medium to a final concentration of 6-200 nM. Single-molecule or confocal imaging was performed within 1 hour after addition of CXCL12.

2.2.4 Calcium assay

The change of the cytoplasmic Ca^{2+} concentration was measured using cell-permeant Fluo4-AM (Invitrogen, USA). Cells were supplemented with 10 μM Fluo4-AM for 30 minutes; prior to imaging the medium in the samples was replaced with fresh IMDM without serum to remove Fluo4-AM from the cells environment. Using time-lapse confocal microscopy

(see below) the Fluo4-AM fluorescence was detected in individual cells with 50 ms laser pulses at 488 nm. Time-lapse imaging of the cells was done with a 100× objective at 5 Hz for 5 minutes. Where indicated, imaging was done with a 10× objective and the fluorescence change was determined for the whole field of view. At a specified time point 100 nM CXCL12 was added and the change in fluorescence intensity inside individual cells was registered.

2.2.5 Actin depolymerization

To induce cytoskeletal actin depolymerization cells were pre-incubated with 500 nM latrunculin B (LatB; Sigma, USA) for 30 minutes, which was sufficient for temporal actin cytoskeleton depletion. Subsequently cells were washed with fresh medium and imaged in serum free IMDM with or without global stimulation. Imaging was performed in a 30 minutes time window after medium change. The actin cytoskeleton was repolymerized within that time (Fig. S1).

2.2.6 Endocytosis inhibition

Endocytosis inhibition was achieved by addition of 25 μM chlorpromazine (CHZ; Sigma, USA), to the cells for 30 min prior to imaging. For imaging the medium was replaced by serum free IMDM and single-molecule or confocal imaging was done in absence or presence of CXCL12.

2.2.7 $G_{\alpha i}$ inhibition

Pertussis toxin (PTX; Sigma, USA) was used to detach $G_{\alpha i}$ from CXCR4. A673-CXCR4 cells were pre-incubated with 200 ng/mL PTX for 5 hours and then single-molecule imaging was done in presence of PTX in the serum free IMDM medium with or without global stimulation.

2.2.8 Single-molecule imaging

For single-molecule imaging we combined wide-field microscopy with high-sensitivity fluorescence microscopy as described in detail earlier (Schmidt et al., 1996). In brief, the sample was mounted onto an inverted microscope (Zeiss, Germany) equipped with a 100× objective

(NA=1.4, Zeiss) and a liquid nitrogen-cooled back-illuminated CCD-camera (Princeton Instruments, USA). A region of interest was set to 40×40 pixels with an apparent pixel size of 202±2 nm. Measurements were done by illumination of the sample with a 514 nm laser beam (Coherent, Germany) for 5 ms at the intensity of 2 kW/cm^2. 1500 images were recorded at 20 Hz. Use of the appropriate filter combination: dichroic: z405/514/647/1064rpc and emission filter: z514/647m (Chroma, USA) permitted the signal detection by the CCD-camera. The x/y positions of individual molecules was determined with a localization precision of $\sigma_{p.a.}$ =35±7 nm (Fig. S2).

Image analysis was done using programs written in MatLab (Mathworks Inc., USA) as described before (Schmidt et al., 1996). Briefly, the signal acquired from individual eYFP molecules was fitted with a 2D-Gaussian and filtered with respect to peak intensity, peak width and detection error thresholds. Subsequently, particle image-correlation spectroscopy analysis, PICS, (Semrau and Schmidt, 2007) was used to calculate the cumulative probability (*cdf*) of squared displacements. The *cdf* revealed that CXCR4 diffusion was not homogeneous and was best described with a model accounting for two or three fractions:

$$cdf_{2fr}(r^2,t) = 1 - \left(\alpha \cdot exp(\frac{-r^2}{MSD_1}) + (1-\alpha) \cdot exp(\frac{-r^2}{MSD_2})\right) \quad (2.1)$$

$$cdf_{3fr}(r^2,t) = 1 - \left(\alpha_1 \cdot exp(\frac{-r^2}{MSD_1}) + \alpha_2 \cdot exp(\frac{-r^2}{MSD_2}) + (1-\alpha_1-\alpha_2) \cdot exp(\frac{-r^2}{MSD_3})\right)$$

where α is the fraction size of the receptors with corresponding characteristic mean square displacement, MSD. The MSD was calculated for different time lags up to 300 ms. Subsequently the MSD was analyzed at different time lags to extract the diffusion coefficient (D):

$$MSD = 4 \cdot D \cdot t_{lag} \quad (2.2)$$

where the offset s_0 is a measure for the localization precision ($s_0 = 4\sigma^2$). For each experimental condition the MSD and α was calculated separately. There was no difference in MSD values between resting and

stimulated cells. Thus the data was re-analyzed jointly, with α as a free parameter. In indicated cases the radius of the confinement, r_{conf}, was calculated as in (Saxton, 1993):

$$MSD(t = \infty) = r_{conf}^2 + s_0 \tag{2.3}$$

2.2.9 Time-lapse microscopy

Time-lapse microscopy was performed using a spinning disk (Yokogawa, Japan) microscope (Zeiss, Germany) equipped with a motorized stage (Maerzhauser, Germany) and a home-built autofocus system facilitating time-lapse imaging at multiple positions. Imaging was done with a 10× or 100× objective (Zeiss, Germany) using brightfield, 488 nm or 514 nm laser illumination at a specified time lag. Image analysis was done using algorithms in MatLab (Mathworks Inc., USA).

2.2.10 Simulation of diffusion on a vesicle

We modeled free diffusion of the receptors with a diffusion coefficient $\mathrm{D}_{CXCR4(vesicle)} = 0.2\ \mu\mathrm{m}^2/\mathrm{s}$ on the surface of a sphere with a diameter $\mathrm{d}_{vesicle} = 150$ nm. Molecules on the sphere were initialised at the positions $p_i = (x_i, y_i, z_i)$ representing a random distribution on the sphere surface. At each time-lag ($\Delta t = 10^{-5}s$) each molecule was displaced to a temporary position $p_i^{'} = (x_i^{'} = x_i + \Delta x_i, y_i^{'} = yi + \Delta y_i, z_i^{'} = z_i + \Delta z_i)$. The displacement in each dimension, i.e.$\Delta x_i, \Delta y_i$ and Δz_i, were assigned an arbitrary length randomly selected from a normal distribution with a width of $\sqrt{MSD} = \sqrt{(2Dt)}$. On this scale the surface of the sphere was considered flat and the displacement of the molecule was taken as a projection of $p_i^{'}$ on the sphere surface by transformation into spherical coordinates, while the r-coordinate was set as equal to the radius of the sphere. Subsequently the new (x_i, y_i, z_i) positions of the molecules were determined as a transformation into cartesian coordinates. Thus, the (x_i, y_i, z_i) positions determined after each Δt represent the displacement of a molecule on the sphere surface. Using the (x_i, y_i) coordinates we calculated the mean square displacement of the molecules in a projection to a plane to mimic the image of moving molecules in a microcope image; $MSD_{sphere-2D}$. Our simulations revealed, that at t = 50 ms $MSD_{sphere-2D}$ was reaching a plateau and the value of the plateau was

determined to be:

$$\lim_{(t\to\infty)} MSD_{sphere-2D}(t) = \frac{4}{3} \cdot R^2_{sphere}$$

2.3 Results

2.3.1 CXCR4-eYFP is functional in A673-CXCR4 cells

We used the Ewing sarcoma-derived cell line A673 (Martinez-Ramirez et al., 2003). For fluorescence imaging of CXCR4 we stably transfected A673 wt cells with DNA encoding for CXCR4-eYFP (further referred to as A673-CXCR4 cells). By visual inspection we estimated the transfection efficiency to be ∼50%. The expression level of CXCR4-eYFP was estimated as described in (de Keijzer et al., 2008). Briefly, the cell's membrane surface was approximated as a spheroid with a short axis of 20 μm and long axis of 50 μm yielding a cell surface area of $\sim 1.1 \times 10^3 \mu m^2$. The fluorescence of CXCR4-eYFP at the apical membrane was detected when illuminated at 2 kW/cm^2 of 514 nm laser beam. The measured signal (35×10^3 cnts/pxl) was divided by the signal predicted for individual eYFP molecules under the same conditions, 220 cnts (Harms et al., 2001; van Hemert et al., 2010). This calculation yielded an average expression level of $(4\pm1)\times10^4$ CXCR4-eYFP molecules per cell, which is within the range of endogenous GPCR expression in mammalian cells (Massotte, 2003). Confocal microscopy showed that CXCR4-eYFP was primarily localized at the plasma membrane (Fig. 2.1A). CXCR4-eYFP was uniformly distributed and did not form any macroscopic domains (Fig. 2.1A, left).

To show that the CXCR4-eYFP was functional and that the fluorescent tag (eYFP) did not alter CXCR4 signaling, we performed functionality assays on the A673-CXCR4 cells. First, we measured intracellular calcium release upon receptor stimulation using the Ca^{2+} reporter Fluo4-AM. Cells were pre-incubated with Fluo4-AM, and subsequently the change in fluorescence signal on global stimulation of the receptors with 100 nM CXCL12 was monitored for individual cells. The increase of the fluorescence intensity of Fluo4-AM corresponds to the increase of cytoplasmic Ca^{2+}. Figure 2.1B shows a representative measurement of the change of fluorescence signal. The shown data were normalized to the signal before cell stimulation. Similar to the results reported (Mueller et al., 2013; Busillo et al., 2010; Venkatesan et al., 2003), stimulation with

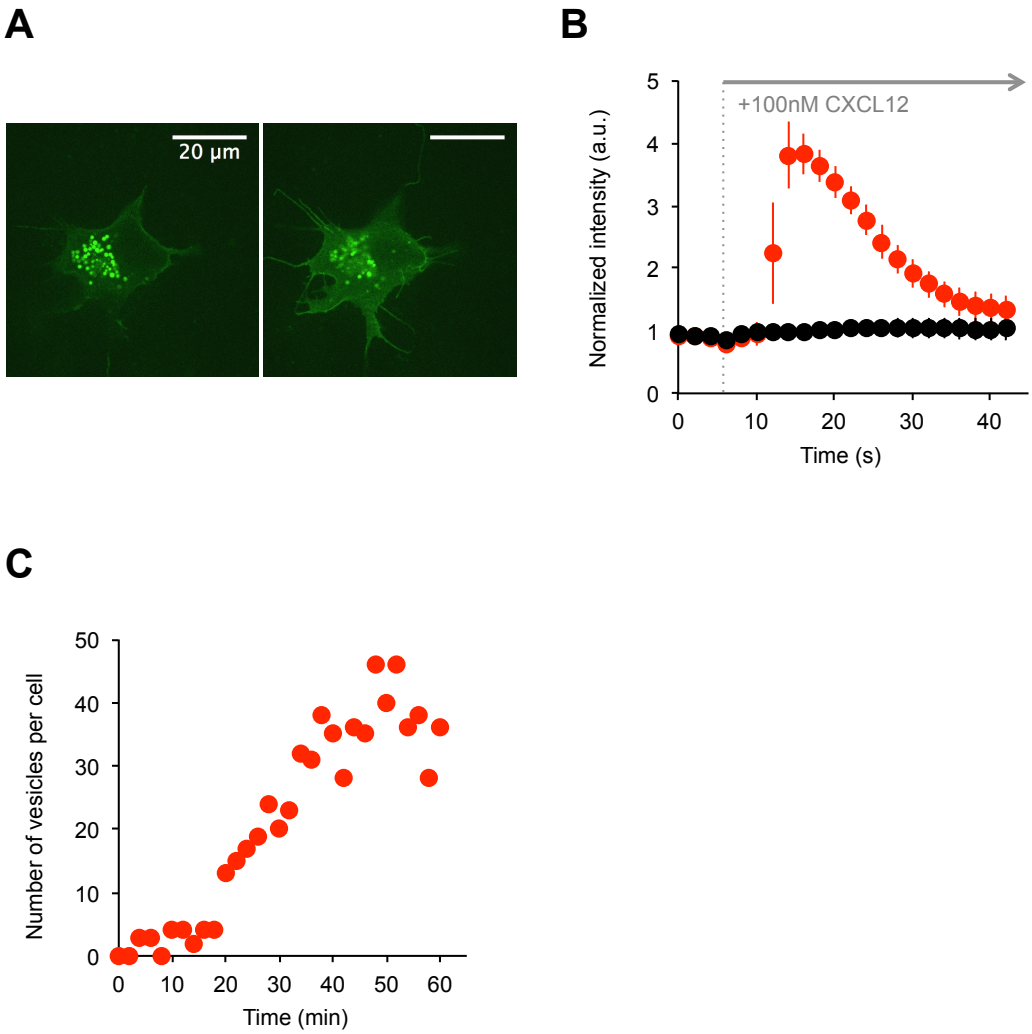

Figure 2.1
Characterization of the A673-CXCR4 cell line. ***A.*** *Confocal images of A673 cells stably transfected with CXCR4-eYFP. The images were acquired by focusing on the basal membrane (left) and in cytoplasmic cross-section of the cell (right).* ***B.*** *Exemplary Ca^{2+} assay measurement. The curves represent the change in fluorescence intensity of the Ca^{2+} indicator - Fluo4-AM - detected in non-transfected cells (black, n=5) or cells transfected with CXCR4-eYFP (red, n=3), after uniform stimulation with 100 nM CXCL12. The error bars represent the standard deviation.* ***C.*** *Appearance of the endocytotic vesicles containing CXCR4-eYFP detected within 60 minutes after cell stimulation with 100 nM CXCL12.*

CXCL12 caused a calcium release, within 20 seconds. Cells expressing CXCR4-eYFP showed a 3.8±0.3 fold intensity increase after receptor stimulation. This result indicates that CXCR4-eYFP were functional and capable of inducing Ca^{2+} release through the respective, $G_{\alpha q}$ pathway.

Another pathway activated shortly after receptor stimulation induces receptor endocytosis. Many GPCRs show internalization via clathrin-dependent endocytosis. Some studies revealed, that upon stimulation CXCR4 internalizes 2 minutes after activation (Venkatesan et al., 2003) and reach a maximum internalization level after ∼30 minutes (Venkatesan et al., 2003; Rey et al., 2007). Therefore, we confirmed that CXCR4-eYFP behaved similarly using 2 minutes time-lapse confocal imaging after CXCL12 addition (Fig. 2.1C). Endocytotic vesicles that contained the fluorescent receptor were manually counted in each frame. Figure 2.1C shows, that after 20 minutes the number of vesicles increased significantly and reached a maximum after 40 minutes. The lack of internalization at an earlier time could be explained (1) by the fact that with confocal imaging only vesicles containing multiple copies of CXCR4-eYFP could be detected; (2) only at a later time the newly formed vesicle detached from the plasma membrane had travelled far enough (∼600 nm) to be distinguishable as entities inside the cell (Serge et al., 2011; Kirchhausen, 2010). This result confirmed that activation with CXCL12 leads to internalization of CXCR4-eYFP, and, hence, the receptor was activating to the β-arrestin pathway.

In summary, we showed that CXCR4-eYFP was properly localized, functional and did not alter the physiological response of the cells. Therefore, we concluded that the A673-CXCR4 cell line was suitable for the study of CXCR4 dynamics and to derive physiological effects.

2.3.2 CXCR4 do not homodimerize upon activation in A673 cells

The biochemical responses of CXCR4 upon stimulation are well established (Teicher and Fricker, 2010). CXCL12 binding to CXCR4 facilitates conformational changes of the receptor leading to the activation of multiple pathways (Teicher and Fricker, 2010). However, knowledge about a possible role of CXCR4 dimerization upon activation is still limited. Earlier reports showed that in 293T cells CXCR4 can be observed in a homodimeric configuration in resting cells and undergos further ho-

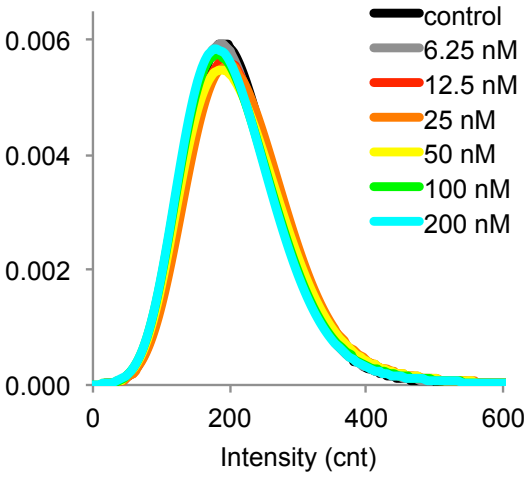

Figure 2.2
Normalized probability density of the intensity of eYFP molecules collected during measurements with or without stimulation. Different colors represent different concentrations of CXCL12.

modimerization upon stimulation with CXCL12 (Springael et al., 2005; Hamatake et al., 2009; Vila-Coro et al., 1999). To test for the presence of homodimers/multimers of CXCR4-eYFP in A673, we analyzed the signal intensity of $>10^5$ YFP signals that were detected on the plasma membrane of transfected cells with and without stimulation by CXCL12 (Fig. 2.2). For individual eYFP molecules at an illumination intensity of 2 kW/cm^2 at 514 nm and an illumination time of 5 ms we expected a signal of ∼220 cnts for individual YPF-molecules (Harms et al., 2001; van Hemert et al., 2010). The appearance of larger signals (>400 cnts) would indicate, that two or more eYFP molecules were detected within the same diffraction limited signal, therefore pointing to receptor dimers or multimers, respectively (Schmidt et al., 1996; Meckel et al., 2011). For resting cells (0 nM) the signal distribution showed only one peak with the maximum at ∼200 cnts (Fig. 2.2, black), corresponding to CXCR4-eYFP monomers. The monomeric distribution did not change upon stimulation with various concentrations of CXCL12 up to 200 nM (Fig 2.2), indicating that CXCR4 stayed monomeric even after activation.

In summary, CXCR4 is a monomeric protein on the plasma membrane of A673 cells independent of its activation state by CXCL12.

2.3.3 Activation of CXCR4 causes immobilization of the receptors

To get deeper insights into the behavior of CXCR4 on the plasma membrane and how it is regulated upon stimulation we applied single-molecule fluorescence microscopy and studied the diffusion dynamics of individual CXCR4-eYFP receptors on the millisecond time-scale at a position accuracy of $\sigma_{p.a.}$=35±7 nm (Fig. S2). A 514 nm laser beam at 2 kW/cm^2 was used in the triggered mode (5 ms illumination) to acquire movies with 1500 frames at a frame-rate of 20 Hz. Each detected fluorescent signal was fit to a 2D-Gaussian (Fig. 2.3A) and filtered with respect to the previously determined eYFP footprint (van Hemert et al., 2010). Subsequently, analysis by particle image correlation spectroscopy, PICS, (Semrau and Schmidt, 2007) was applied to construct the cumulative probability density functions (*cdf*) of square displacement for various time lags. Our results revealed that in resting cells the *cdf* were best described with a model accounting for two fractions, a mobile receptor fraction and an immobile receptor fraction (Fig. S3A, green line). The fraction size (α) and mean square displacements (MSD_1 and MSD_2) were calculated according to eq.(2.1) for various time lags from 50 ms up to 300 ms. The change of MSD_1 and MSD_2 varied with the time lag as shown in Figure 2.3B. MSD_2 did not change over time and was equal to 0.013±0.001 μm^2. It is important to note that the value of MSD_2 was significantly larger than that predicted for an immobile receptor of $4\sigma^2_{p.a.}$= 0.005±0.001 μm^2. This indicates that processes at a shorter time scale (<50 ms), which we could not detect with our imaging settings were responsible for this initial increase. Nonetheless, for brevity, we further refer to the receptor fraction with MSD_2 as immobile.

MSD_1 showed a linear dependence on the time lag as predicted for free diffusion (Fig. 2.3B). Fitting according to eq.(2.3) yielded D_{CXCR4}= 0.18±0.01 μm^2/s. This value is in good agreement with the diffusion coefficient determined, e.g. for the cAMP-receptor in Dictyostelium (0.17±0.02 μm^2/s) (de Keijzer et al., 2008) or other GPCRs in mammalian cells (Calebiro et al., 2013; Lill et al., 2005). The fraction of mobile receptors comprised α=81±3% of the receptors (Fig. 2.3, black)

To study how the activation of CXCR4 influences the behavior of the receptor on the plasma membrane, we applied global stimulation of the cells with CXCL12. CXCL12 was added to the cells right before imaging and single-molecule data were collected within the following hour. Up to

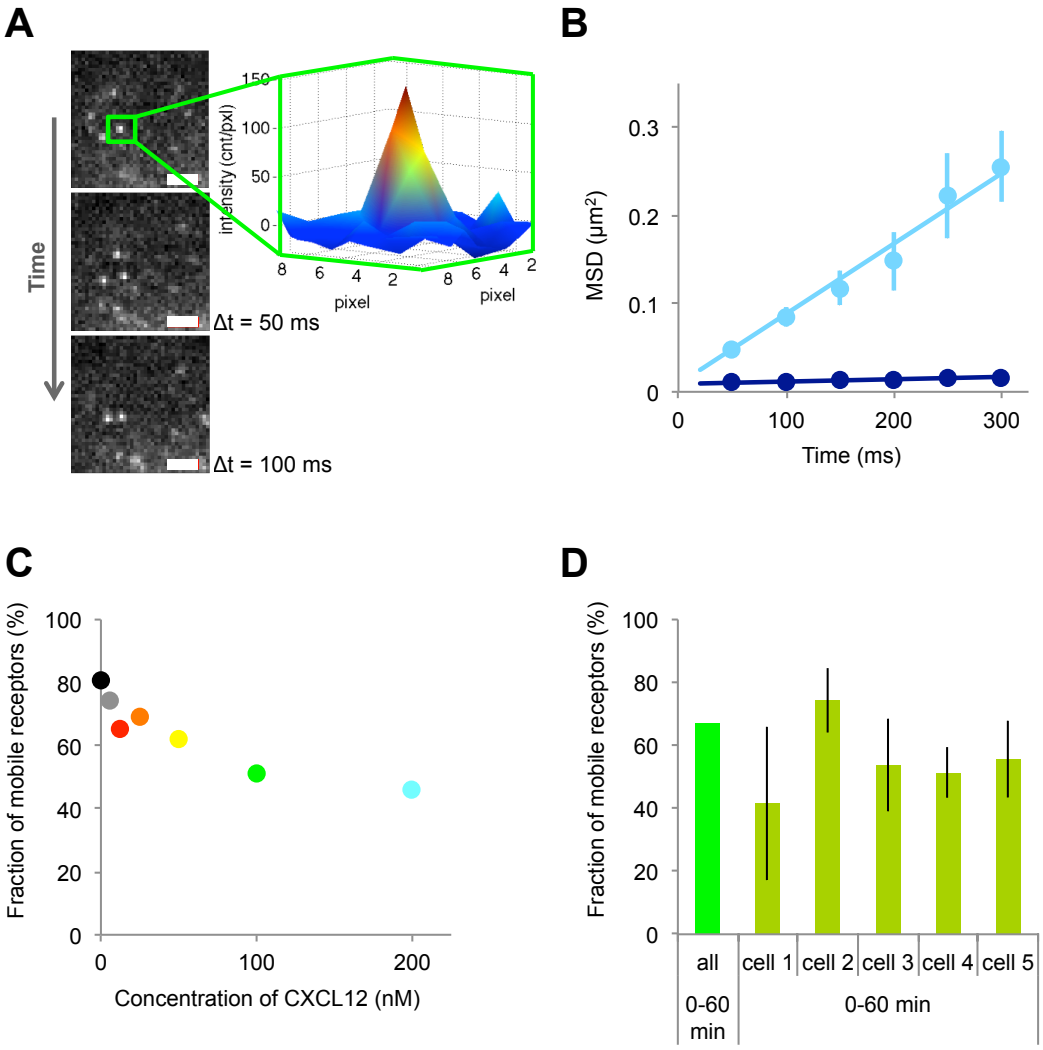

Figure 2.3

Single-molecule characterization of CXCR4 diffusion in resting cells and upon global stimulation with CXCL12. ***A.*** *Single-molecule imaging scheme. Scale-bar: 2 μm.* ***B.*** *Mean square displacement (MSD) vs time plot. MSD of mobile (blue) and immobile (purple) receptors as resulting from a simultaneous fit of the resting and CXCL12 stimulated cells' data sets.* ***C.*** *Dependence of the mobile receptor fraction on the CXCL12 concentration. The color-code correspond to the one used in Figure 2.2.* ***D.*** *The mobile receptor fraction detected at different time points after addition of 100 nM CXCL12 within one experiment. Cell1-cell5 represents five individual cells imaged subsequently within one experiment (0-60 min). 'All' represent the mobile receptor fraction detected by simultaneous analysis of all cells imaged within one experiment.*

five cells were imaged sequentially during one experiment. Each cell was taken as a representative of a 10-15 minutes time window after CXCL12 addition. At least 20 cells were imaged per condition. As shown in Figure 2.3D the mobile receptor fraction size (α) detected for every individual cell during activation exhibited a similar value as for the following cells. The mobile receptor fraction determined from simultaneous analysis of all cells within the experiment (Fig. 2.3D, All) exhibited the same value as that of an individual cells. This result suggests that receptor stimulation had a long-lasting effect on the receptor mobility and did not change over time within 60 min.

Our results showed a strong correlation between receptor stimulation and receptor mobility in a concentration-dependent manner. Addition of increasing concentrations of CXCL12 systematically shifted the cumulative probability distribution of square displacements to lower values (Fig. S1B). The shift in the *cdf* was attributed to a redistribution of the receptor fractions. As shown in Figure 2.3C, the mobile receptor fraction decreased from ∼80% (no CXCL12) to ∼45% (200 nM CXCL12) in a CXCL12 concentrations-dependent manner. This finding was in agreement with earlier findings for other GPCRs (Lill et al., 2005; Jacquier et al., 2006). It is noteworthy that an increase in receptor mobility has been found for cAMP-receptor in Dictyostelium (de Keijzer et al., 2008) and for GABAB in HEK293 cells (Calebiro et al., 2013).

In summary, our results showed that CXCR4 on the plasma membrane is either freely diffusing or immobile. CXCR4 is immobilized upon stimulation with CXCL12 in a concentration-dependent manner.

2.3.4 Actin cytoskeleton is not responsible for CXCR4 immobilization

Many studies agree that GPCR dynamics is actin-cytoskeleton regulated (Andrews et al., 2008; Luo et al., 2006; Tsao et al., 2001; Papadopoulou et al., 2009). Thus, we decided to test whether the actin cytoskeleton underlining the plasma membrane could be involved in modulation of CXCR4 mobility. For this purpose, we induced actin depolymerization by Latrunculin B (LatB). Pre-incubation with LatB for 30 minutes was sufficient to effectively deplete actin (Fig. S1). LatB induces only temporal actin-cytoskeleton depolymerization. Thus, we analyzed the data acquired within the first 30 minutes after medium exchange, while the data collected at 30-60 minutes after which the membrane-skeleton was

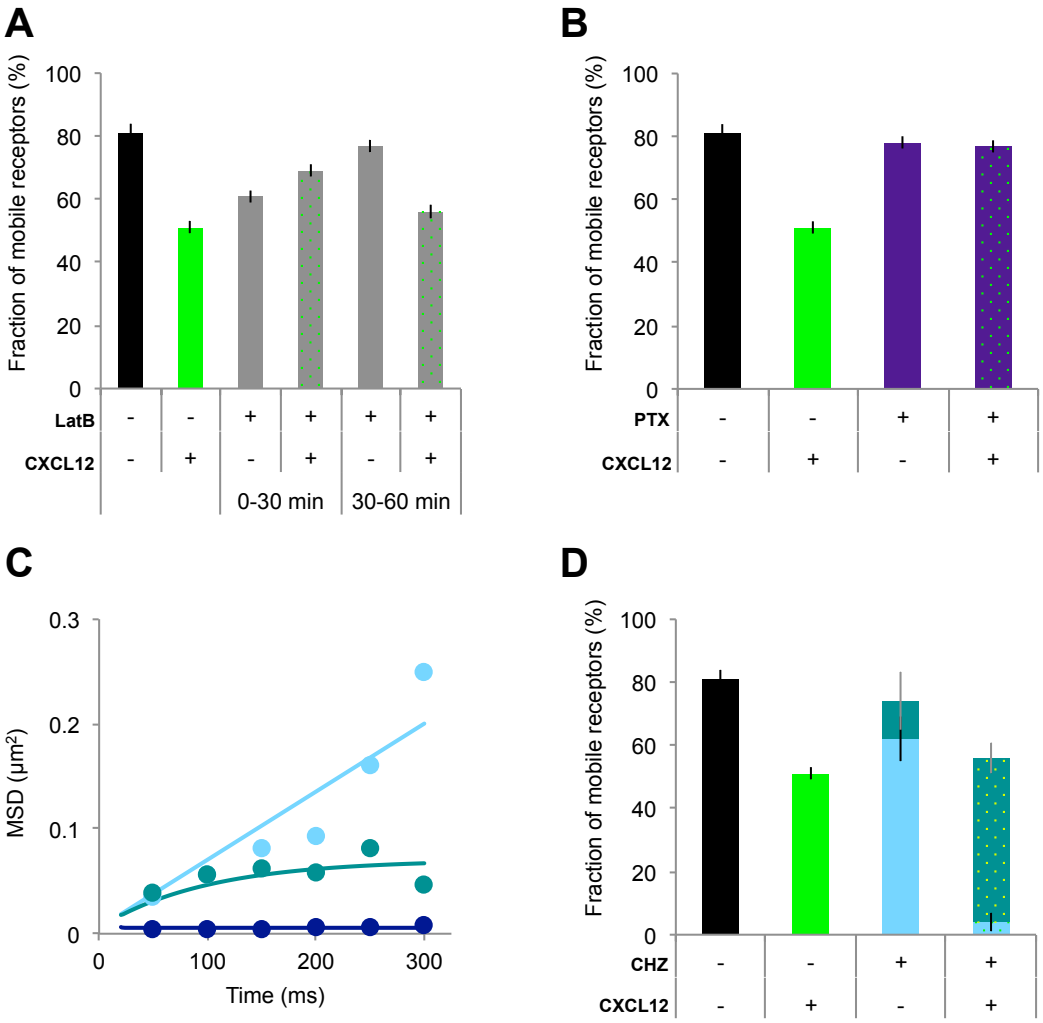

Figure 2.4

Effect of different drug treatments. ***A.*** *The fraction of mobile CXCR4-eYFP in cells pre-treated with LatB (grey) without or with (green punctate pattern) global stimulation by 100 nM CXCL12, compared to the mobile receptor fraction measured in control cells without (black) and with (green) stimulation. LatB provided temporal actin depletion, therefore the acquired data was split accordingly: 0-30 min and 30-60 min.* ***B.*** *Fraction of mobile CXCR4-eYFP measured in PTX pre-treated (purple) cells without and with (green punctate pattern) activation, compared to control cells without (black) and with (green) uniform stimulation with 100 nM CXCL12.* ***C.*** *The MSD vs time plot of the immobile (purple), confined (green) and freely mobile (blue) receptors measured in CHZ pre-treated cells. Solid lines represent the respective fit of the data. The size of the confinement zone was estimated from the linear fit to the plateau and yielded* $r_{conf} = 236 \pm 6$ *nm.* ***D.*** *The mobile receptor fraction in CHZ treated cells presented by two sub-fractions of mobile receptors: freely diffusing (light blue) and confined (dark green). Uniform admission of 100 nM CXCL12 (green punctate pattern) caused a drastic change in the ratio of mobile subpopulations. The total size of the mobile fraction in CHZ pre-treated cells was comparable to the one in the control cells without (black) or with (green) CXCL12 admission.*

re-established served as a control.

To our surprise actin depolymerization did not lead to an increase of the mobile receptor fraction but rather to a decrease to ∼61% (Fig. 2.4A, 0-30 min) in non-stimulated cells. Receptor activation with 100 nM CXCL12 slightly changed the mobile receptor fraction to 69% (Fig. 2.4A, 0-30 min). Data collected after actin repolymerization (30 min after medium exchange) replicated the results acquired for cells with intact actin cytoskeleton (Fig. 2.4A, 30-60 min). In resting cells, the fraction of the mobile receptors reached 77±2% and in the cells stimulated with CXCL12, it dropped to 56±2%.

In summary, our results suggest that in resting cells with intact actin skeleton, the immobile CXCR4 receptors were not anchored to the actin cytoskeleton. Activation by CXCL12 induced an actin-dependent process promoting CXCR4 immobilization. Thus, our result suggests that actin might have an indirect effect on CXCR4 regulation which will be discussed later.

2.3.5 CXCR4 in endocytotic vesicles contribute to the immobile receptor fraction

Upon stimulation many GPCRs proceed to internalization (Tsao et al., 2001; Schwartz et al., 2012; Teicher and Fricker, 2010). Activated GPCRs are known to bind to β-arrestin, which in turn links them to the AP2 adapter complex (Vassilieva and Nusrat, 2008) and facilitates their clathrin-dependent endocytosis. Given that CXCR4 is known to internalize via clathrin-dependent endocytosis upon stimulation and, at the same time, to undergo constitutive internalization without stimulation (Bhandari et al., 2007), we further hypothesized that receptor internalization could possibly explain the drop of the mobile CXCR4 receptor fraction upon stimulation. For the experiments we used chlorpromazine (CHZ), an inhibitor of clathrin-dependent endocytosis. CHZ causes loss of clathrin from the cell surface in the coated pits and, therefore, prevents formation of new clathrin-coated vesicles (CCVs) (Wang et al., 1993; Stuart et al., 2006). Effect of CHZ is very cell-type dependent (Vercauteren et al., 2010). For A673-CXCR4 cells 30 min incubation with 25 μM CHZ was sufficient to inhibit clathrin-dependent endocytosis of CXCR4 effectively, while not causing dramatic cytotoxicity (data not shown).

Single-molecule imaging revealed that CHZ pre-treated cells exhib-

ited the same mobile CXCR4 receptor fraction (α = 74±9%) as control cells (α = 81±3%). However, in the CHZ pre-treated cells the mobile receptor fraction was composed of two sub-fractions, a freely diffusing fraction (62±7%) and a receptor fraction that exhibited confined diffusion (12±9%) as reflected by a sub-linear increase of MSD with timelag (Fig. 2.4C,D). Both sub-fractions of mobile receptors showed similar diffusion coefficients as the fraction of mobile receptors in resting cells, DCXCR4 (CHZ) = 0.16±0.02 μm^2/s. The size of the confinement zone was estimated from a fit to the plateau in the MSD vs time plot (Fig. 2.4C) according to eq.(2.3) in Materials and Methods and yielded r_{conf} = 236±6 nm.

Given the typical radius of a clathrin-coated vesicle of ∼75-100 nm (McMahon and Boucrot, 2011), which contains a surface area of 0.07-0.13 μm^2 equal to the area covered by the confinement zone in our experiments, we suggest that receptors exhibiting confined diffusion correspond to the receptors trapped in a pre-cursor structure of clathrin-coated pits. Thus, in CHZ pre-treated cells mobile receptors undergoing constitutive internalization accumulate in a precursor structure of clathrin-coated pits and stay locked there since endocytosis cannot proceed.

When CHZ pre-treated cells were stimulated with 100 nM CXCL12, the fraction of mobile receptors decreased (α = 56± 6%) and the distribution of receptors between freely diffusing and confined fractions changed dramatically (Fig. 2.4D). Nearly all receptors showed confined diffusion, while only a small fraction showed free diffusion (52±5% and 4±3%, respectively), suggesting that activated receptors proceed to internalization. This is in good agreement with our internalization experiment (Fig. 2.1C) and with data from other groups (Venkatesan et al., 2003; Rey et al., 2007), showing that upon stimulation the rate of CXCR4 internalization increases.

In summary, CHZ prevents the formation of clathrin-coated vesicles and, hence, receptors proceeding to internalization get trapped in confined areas reminiscent of precursor structures of coated pits. Thus, our results suggest, that the immobile fraction of receptors upon stimulation was caused by CXCR4 trapped in clathrin-coated vesicles, in which the diffusion could not be resolved (see below).

2.3.6 G-proteins control CXCR4 immobilization

Up to date, internalization of GPCR's is considered as a way of receptor desensitization. Our results, suggest that internalizing receptors appear as immobile. However, the ratio of mobile and immobile fractions in stimulated CHZ pre-treated cells resembled such of the control cells. At the same time we find that immobilization of CXCR4 correlated with activation of receptors. Therefore, having established a correlation between receptor mobility and signaling, we were interested in how receptor mobility is affected when the signaling chain is disrupted at the level of G-proteins. Previous reports showed a change in G-protein mobility while the cAR1 receptor was stimulated (van Hemert et al., 2010). Stimulation of CXCR4 mainly results in activation of two isoforms of the G_{α} subunit: $G_{\alpha q}$ and $G_{\alpha i}$ (Teicher and Fricker, 2010). Kleemann et al. showed elevated coupling of $G_{\alpha i}$ to CXCR4 upon receptor stimulation (Kleemann et al., 2008). This coupling of the $G_{\alpha i}$ on the cytosolic side should not per se influence the receptor dynamics. However, hypothesizing that the $G_{\alpha i}$ pathway activation might result in formation of a supramolecular scaffold (Ritter et al., 2009) for further signalling, we probed how the interaction of CXCR4 with the $G_{\alpha i}$ subunit could modulate the mobile receptor fraction.

In our experiments we used pertussis toxin (PTX) as an agent resulting in loss of coupling of $G_{\alpha i}$ and the receptor (Moss et al., 1984; Mangmool and Kurose, 2011). We pre-incubated A673-CXCR4 cells with PTX for 5 hours. During the experiments PXT was also present in the medium. As predicted, in resting cells, single-molecule imaging of CXCR4-eYFP did not show any change in the diffusion coefficient of the receptors. Moreover, the mobile receptor fraction did not change compared to the control without PXT (Fig. 2.4B), suggesting that if $G_{\alpha i}$ was coupled to CXCR4 it had no measurable impact on the receptor dynamics. However, when 100 nM CXCL12 was added to the cells, no significant drop in the mobile receptor fraction was observed (Fig. 2.4B). This behavior was in contrast to the decrease in the mobile receptor fraction detected for CXCR4 receptors upon stimulation in control cells (Fig. 2.4B, green bar). This result supports our earlier conclusion that a bigger fraction of immobile receptors is strongly correlated to receptor signalling.

In summary, our results imply that the decrease in the mobile receptor fraction upon stimulation must be interpreted as an outcome of the

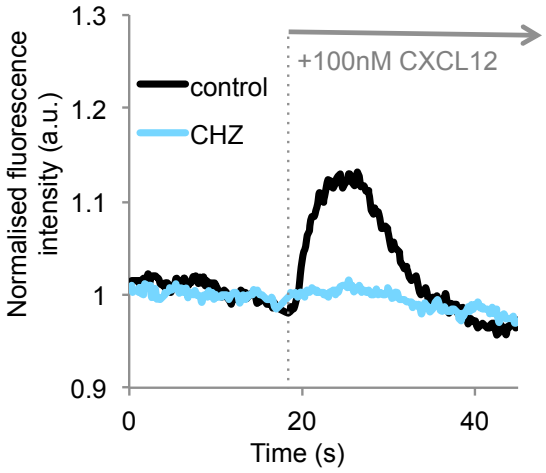

Figure 2.5
Ca^{2+} assay. The curves represent the change in fluorescence intensity of the Ca^{2+} indicator - Fluo4-AM - detected in cells pre-treated with CHZ (light blue) or in control (black) cells after uniform stimulation with 100 nM CXCL12.

of the subsequent $G_{\alpha i}$-pathway activation potentially resulting in formation of a supramolecular scaffold (signalosome, see Fig. 2.6), while blocking the receptor interaction with $G_{\alpha i}$ lead to receptor mobility that did not change upon stimulation.

2.3.7 Cross-talk between G-protein dependent and independent pathways

Our results showed, that immobilization of CXCR4 upon stimulation is facilitated via receptor endocytosis. At the same time the $G_{\alpha i}$-dependent pathway also lead to CXCR4 immobilization. Taken together, these results suggest that G-protein dependent and independent pathways are cross-regulated. Thus, we checked whether a G-protein dependent pathway would be affected by inhibition of CXCR4 endocytosis. We performed a Ca^{2+} assay in the cells under different conditions. Cells with inhibited clathrin-dependent endocytosis (pre-treated with CHZ) showed no Ca^{2+} release upon CXCR4 activation (Fig 2.5). This result implies, that the G-protein independent pathway of receptor internalization was interfering with the early stages of a G_{α}-dependent pathway.

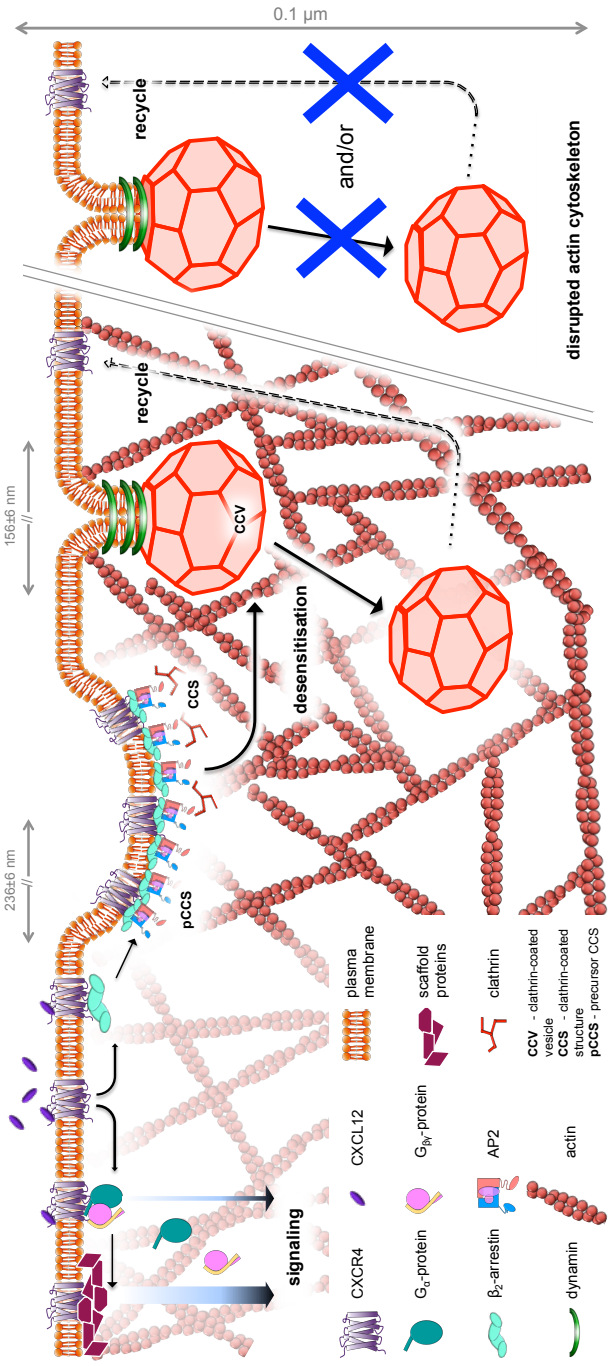

Figure 2.6
Current model. Binding with CXCL12 CXCR4 is activating G-protein dependent (left) and independent (right) pathways. Activation of the biochemical pathways result in CXCR4 immobilization either in super-molecular signalosome, causing enhanced signalling, or in the clathrin-coated vesicles, resulting in receptor internalization, imply a cross-talk between these signalling cascades.

In summary, we suggest that two processes together regulate CXCR4 mobility and thus activation/signalling. Endocytosis driven immobilization leads to desensitization while G-protein driven local signalosome formation might result in signal enhancement (Fig. 2.6). Together, both processes regulate the overall cellular response.

2.4 Discussion

GPCR signalling is a complex process in which only parts have been unraveled. Activation of CXCR4 promotes signalling through G-proteins resulting in expression of certain genes, cells survival/proliferation, chemotaxis, etc. Simultaneously G-protein independent pathways, e.g. β-arrestin, are activated and result in receptor desensitization (Teicher and Fricker, 2010). All the biochemical pathways are studied in detail, but the role of the receptor dynamics on the plasma membrane remains poorly understood.

To elucidate the molecular mechanism of CXCR4 signal transduction, we studied CXCR4 during activation using the receptor mobility as a marker. Our results revealed that already in the resting cells receptor diffusion was not homogeneous. We detected two receptor species, one mobile and one immobile. Activation of CXCR4 with CXCL12 caused a concentration-dependent decrease of the mobile receptor fraction, indicating a correlation between receptor signalling and diffusion on the plasma membrane. Our data gives information on receptor diffusion at millisecond time scales, while, most biochemical or other receptor-signalling processes require longer time, e.g. endocytosis of a receptor takes $\sim$1 minute (Cocucci et al., 2012; Boulant et al., 2011). In this respect, our results depict a snapshot. However, we did not observe a time dependent change in the mobile receptor fraction (Fig. 2.3D), meaning that there was a constitute fraction of immobile receptors.

Many studies of GPCRs agree that receptors dynamics/signalling strongly depends on the actin cytoskeleton. Actin remodelling was reported to have a key role in the pro-apoptotic responses upon mAR activation (Papadopoulou et al., 2009). Luo et al. showed that a big portion of CXCR4 is pre-coupled with the cortical actin binding protein - cortactin (Luo et al., 2006). Stimulation with CXCL12 induced further translocation of cortactin from endosomal compartments and colocalization with CXCR4. However, our results did not show actin-dependent

changes in the diffusion coefficient of CXCR4, and actin depletion did not cause the predicted increase in receptor mobility. In contrast, in the actin depleted cells the fraction of mobile receptors was decreased compared to control. These results imply that there is no direct physical interaction between receptors and actin. However, the change in the CXCR4 mobile fraction indicated, that there was actin-dependent regulation of receptor mobility.

Actin is known to play an important role in sorting of GPCRs to diverse membrane pathways after endocytosis (Tsao et al., 2001; Samaj et al., 2004). For instance, linking of the β2-adrenoreceptor to actin inhibits trafficking of endocytosed receptors to lysosomes and promotes their recycling to the plasma membrane (Tsao et al., 2001). Therefore, during actin cytoskeleton depletion one could expect that most of the receptors, which are endocytosed, follow the lysosomal route instead of being recycled to the plasma membrane (Fig. 2.6, right side). Such a process could lead to a change in the balance of different fractions of receptors present on the plasma membrane. Moreover, there are indications that actin is involved in all forms of endocytosis (Samaj et al., 2004). Though, actin was reported to function as a late component of clathrin-dependent endocytosis (McMahon and Boucrot, 2011) it is responsible for a range of processes (Kichhausen, 2009). EM imaging and life-cell imaging showed that depletion of the actin cytoskeleton caused an increased fraction of shallow and curved clathrin-coated structures on the plasma membrane in comparison to invaginated structures and formed vesicles (Yarar et al., 2005; Boulant et al., 2011). Furthermore, it was shown that actin polymerization at the plasma membrane controls both the alignment and mobility of clathrin-coated vesicles, facilitates the internalization step, and drives rapid transport of early endosomes away from the plasma membrane in the cytosol (Samaj et al., 2004). Hence, actin depletion can be considered as one form of indirect clathrin-dependent endocytosis inhibition at a later stage. Accordingly, in actin-depleted resting cells, CXCR4 undergoing constitutive internalization stall in vesicles, which cannot be removed from the plasma membrane (Fig.2.6, right side). These receptors contribute to the observed immobile fraction (see below). During receptor activation, disturbed vesicle formation and/or vesicle scission could result in CXCR4 failing to proceed with endocytosis and to show the accompanying decrease in the mobile receptor fraction.

In our experiments we used CHZ to directly address the question of

how endocytosis interferes with the mobility of CXCR4 on plasma membrane. CHZ causes loss of clathrin from the cell surface in the coated pits and, therefore, prevents formation of new clathrin-coated vesicles (CCVs) (Wang et al., 1993; Stuart et al., 2006). However, loss of clathrin from the cell surface would not affect the early stages of clathrin-coated structure (CCS) formation. Clathrin-coated vesicle formation consists of five steps: (1) nucleation, (2) cargo selection, (3) coat assembly, (4) scission and (5) uncoating (McMahon and Boucrot, 2011). The first two steps are promoted by a number of initiation proteins, e.g. FCHO 1,2, Epsin and adaptor proteins, e.g. β-arrestin. These proteins result in initiation of the membrane curvature and receptor recruitment (Fig.2.6 middle). Further, the AP2 adaptor protein and clathrin are recruited during clathrin-coated pit maturation and coat assembly. Thus, a membrane invagination appears and progresses before recruitment of clathrin (McMahon and Boucrot, 2011). Therefore, CHZ pre-treated cells could still form precursor structures of clathrin-coated pits (pCCS), while further internalization was blocked. This mechanisms of the endocytosis inhibition is favorable when addressing the endocytosis-mediated regulation of the receptor dynamics on the plasma membrane. Our data showed, that inhibition of a clathrin-dependent endocytosis with CHZ caused appearance of a receptor fraction undergoing confined diffusion. During CXCR4 activation in CHZ pre-treated cells all mobile receptors were diffusing in a confinement zone. The radius of the confinement zone (236±6 nm) suggested that the confinement corresponded to precursor CCS (pCCS). Upon stimulation CXCR4 was driven to CCVs, but due to the CHZ pre-treatment, the receptors were confined to pCCS.

Thus, in untreated cells CXCR4 would be trapped in CCVs after stimulation. As the typical size of a CCV equals 100-200 nm which is within the axial resolution of our microscope (∼1 μm) (Fig.2.6), diffusion of the receptors on the vesicle surface will be detected as a 2D projection . To elucidate the effect hereof, we modeled free diffusion of the receptor on a vesicle with a diffusion coefficient $D_{CXCR4(vesicle)}$=0.2 $\mu m^2/s$ on the surface of a vesicle with a diameter $d_{vesicle}$= 150 nm and subsequently analyzed the 2D-projection of the data. Our simulations revealed, that the $MSD_{sphere-2D}$ linearly increased with timelag and reached a plateau at a time lag of t = 50 ms (Fig. S4), which corresponds to the time lag of our single-molecule measurements. The simulations further revealed that the plateau value is given by $MSD_{(sphere-2D)}(t = \infty) = \frac{4}{3}R^2$,

where R is the vesicle radius. Further, taking into account the positional accuracy of $\sigma_{p.a.}$ = 35±7 nm, and the value we found for MSD_2, σ_{MSD2} = 57±2 nm, the vesicle radius is then given by $\frac{4}{3}R^2_{MSD2} = 4\sigma^2_{MSD2} - 4\sigma^2_{(p.a.)}$. Using our experimental findings we calculated a value R_{MSD2} = 78±3 nm which was very similar to the size of a clathrin-coated vesicle. Together these findings showed that the immobile receptors we found can be attributed to receptors diffusing in a CCV. Thus, CXCR4 undergoing constitutive internalization (Bhandari et al., 2007) would contribute to the immobile receptor fraction in resting cells and the increase of the immobile fraction during activation would be related to an elevated level of clathrin-dependent endocytosis of CXCR4. Hence, clathrin-dependent endocytosis is involved in regulation of CXCR4 mobility on the plasma membrane.

Stimulation experiments showed a concentration-dependent decrease of the mobile receptor fraction, indicating that receptor immobilization was correlated with CXCR4 activation. This was further confirmed by experiments in cells treated with PTX. Detachment of $G_{\alpha i}$ from CXCR4 altered the ratio of mobile to immobile receptors in response to CXCL12 stimulation, compared to non-treated cells. There was no decrease in the mobile receptor fraction, supporting our hypothesis of correlated CXCR4 mobility on the plasma membrane and signalling. As clathrin-dependent endocytosis is G-protein independent and the majority of biochemical signalling of CXCR4 is mediated through activation of the $G_{\alpha i}$-subunit, PTX is a tool to separate G-protein dependent and independent pathways. In contrast to neuroblastoma cells, where $G_{\alpha i}$ detachment with PTX failed to inhibit internalization of CXCR4 upon CXCL12 addition (Clift et al., 2014), our experiments suggest that in Ewing sarcoma cells, disrupted receptor signalling prevented receptor internalization. This idea is supported by the number of reports claiming an important role of caveolin (main component of caveolin-dependent endocytosis; Pelkmans and Helenius, 2002) in signalling of various molecules in Ewing sarcoma (Martins et al., 2011; Sainz-Jaspeado et al., 2010; Tirado et al., 2006; Sainz-Jaspeado et al., 2013). For instance, it was shown that in Ewing sarcoma cells blockade of IGF1R endocytosis inhibits the receptor's signalling (Martins et al., 2011). Furthermore, in our experiments, CHZ pre-treatment disturbed $G_{\alpha q}$-dependent Ca^{2+} release upon CXCL12 stimulation.

In conclusion, here we showed that in Ewing sarcoma derived A673

cells the CXCR4 receptor mobility on the plasma membrane is strongly correlated with receptor signalling. Activated receptors are immobilized in a concentration-dependent manner. Immobilization of the receptor is facilitated via clathrin-dependent endocytosis structures, e.g. vesicles, or via $G_{\alpha i}$ - initiated supramolecular scaffolding. Inasmuch as these processes lead to opposite results (desensitization or signal enhancement in signalosomes, respectively) balanced regulation of G-protein dependent and independent pathways is required for proper receptor signal transduction.

2.5 Supplemental figures

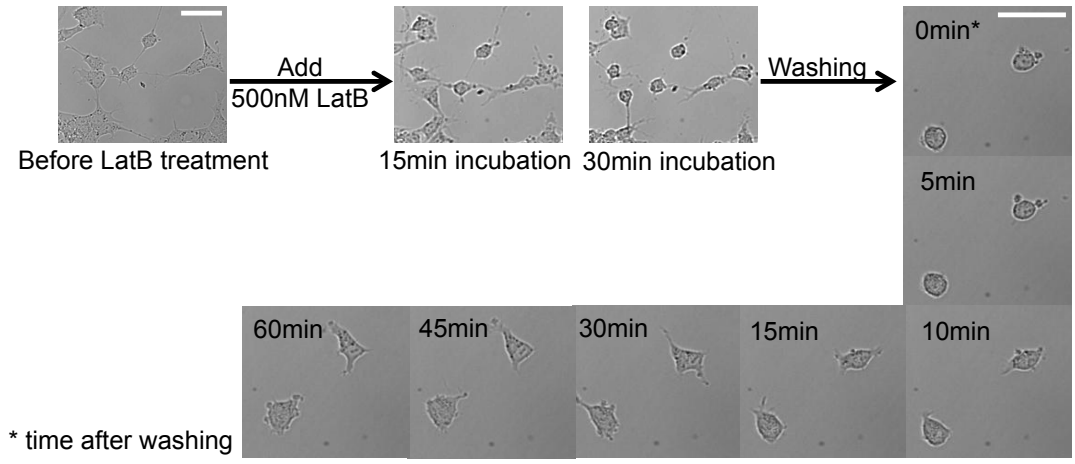

Figure S1
LatB treatment. Cells pre-treated with 500 nM LatB for 30 min loose their shape and show round morphology. After media change actin stays depleted for up to 30 min, subsequently actin was repolymerized. Scale bar: 50 μm.

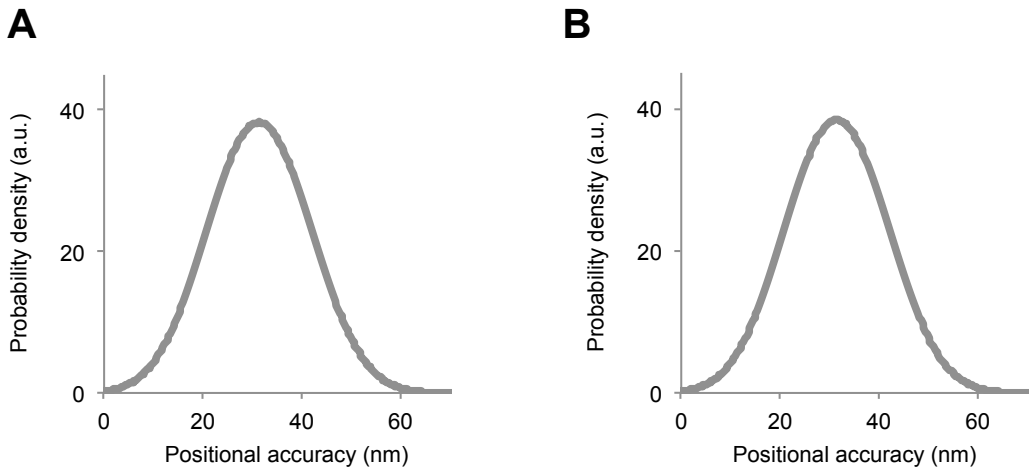

Figure S2
*Positional accuracy of single molecules in x (**A**) and y (**B**). The data was collected for over 10^5 molecules and thresholded with respect to the signal width and intensity.*

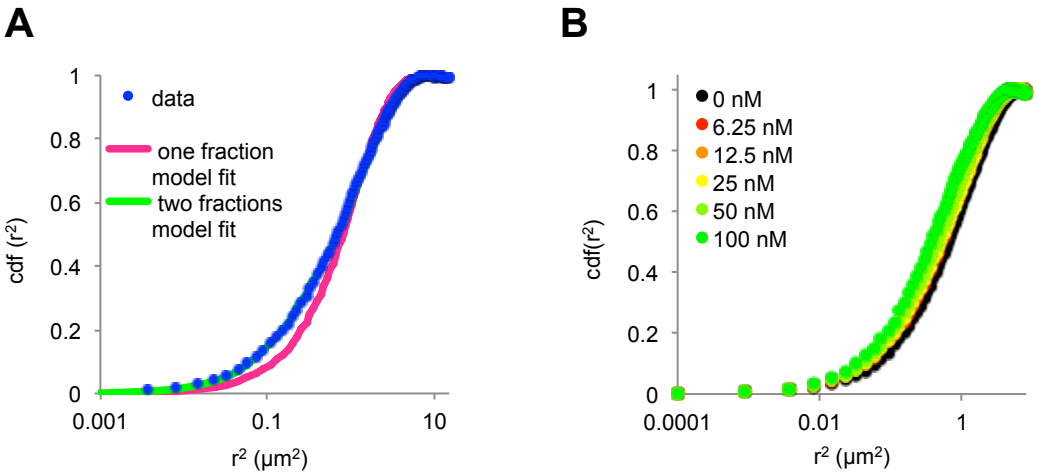

Figure S3

A. *Cumulative distribution of square displacements in resting (control) cells. Data points (blue dots) were best fit with a two fraction model (green curve), while a one fraction model (pink curve) failed.* ***B.*** *Cumulative distribution of square displacements of CXCR4-eYFP constructed for the cells with uniform admission of different concentrations of CXCL12 - from ∼6 nM (red) to 100 nM (green) - are shifted compared to the cdf without stimulation (black).*

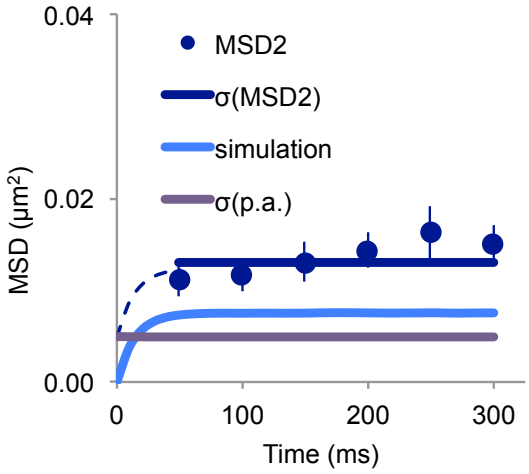

Figure S4

Simulation of the free diffusion on the vesicle compared to MSD_2 data and positional accuracy. Dashed line is a result of summation of simulation and positional accuracy for 50 ms.

2.6 Acknowlegement

We thank S. Coppola for help with the data analysis, Karoly Szuhai and Laurens Sand for the valuable comments on data interpretation.

2.7 References

Andrews, N. L., Lidke, K. A., Pfeiffer, J. R., Burns, A. R., Wilson, B. S., Oliver, J. M. and Lidke, D. S. (2008). Actin restricts FcepsilonRI diffusion and facilitates antigen-induced receptor immobilization. Nat Cell Biol. 10, 955-963.

Bennani-Baiti, I. M., Cooper, A., Lawlor, E. R., Kauer, M., Ban, J., Aryee, D.N. and Kovar, H. (2010). Intercohort gene expression co-analysis reveals chemokine receptors as prognostic indicators in Ewing's sarcoma. Clin Cancer Res. 16, 3769-3778.

Berghuis, D., Schilham, M. W., Santos, S. J., Savola, S., Knowles, H. J., Dirksen, U., Schaefer, K. L., Vakkila, J., Hogendoorn, P. C. and Lankester, A. C. (2012). The CXCR4-CXCL12 axis in Ewing sarcoma: promotion of tumor growth rather than metastatic disease. Clin Sarcoma Res. 2, 24.

Bhandari, D., Trejo, J., Benovic, J. L. and Marchese, A. (2007). Arrestin-2 interacts with the ubiquitin-protein isopeptide ligase atrophin-interacting protein 4 and mediates endosomal sorting of the chemokine receptor CXCR4. J Biol Chem. 282, 36971-36979.

Boulant, S., Kural, C., Zeeh, J. C., Ubelmann, F. and Kirchhausen, T. (2011). Actin dynamics counteract membrane tension during clathrin-mediated endocytosis. Nat Cell Biol. 13, 1124-1131.

Busillo, J. M. and Benovic, J. L. (2007). Regulation of CXCR4 signaling. Biochim Biophys Acta. 1768, 952-963.

Calebiro D., Rieken, F., Wagner, J., Sungkaworn, T., Zabel, U., Borzi, A., Cocucci, E., Zurn, A. and Lohse, M. J. (2013). Single-molecule analysis of fluorescently labeled G-protein-coupled receptors reveals complexes with distinct dynamics and organization. Proc Natl Acad Sci U S A. 110, 743-748.

Clift, I. C., Bamidele, A.O., Rodriguez-Ramirez, C., Kremer, K. N. and Hedin, K. E. (2014). β-Arrestin1 and distinct CXCR4 structures are required for stromal derived factor-1 to downregulate CXCR4 cell-surface levels in neuroblastoma. Mol Pharmacol. 85, 542-552.

Cocucci, E., Aguet, F., Boulant, S. and Kirchhausen, T. (2012). The first five seconds in the life of a clathrin-coated pit. Cell. 150, 495-507.

de Keijzer, S., Serge, A., van Hemert, F., Lommerse, P. H., Lamers, G. E., Spaink, H. P., Schmidt, T. and Snaar-Jagalska, B. E.. (2008). A spatially restricted increase in receptor mobility is involved in directional sensing during Dictyostelium discoideum chemotaxis. J Cell Sci. 121,

1750-1757.

Decaillot, F. M., Kazmi, M. A., Lin, Y., Ray-Saha, S., Sakmar, T. P. and Sachdev, P. (2011). CXCR7/CXCR4 heterodimer constitutively recruits beta-arrestin to enhance cell migration. J Biol Chem. 286, 32188-32197.

Hamatake, M., Aoki, T., Futahashi, Y., Urano, E., Yamamoto, N. and Komano, J. (2009). Ligand-independent higher-order multimerization of CXCR4, a G-protein-coupled chemokine receptor involved in targeted metastasis. Cancer Sci. 100, 95-102.

Harms, G. S., Cognet, L., Lommerse, P. H. M., Blab, G. A., Kahr, H., Gamsjager, R., Spaink, H. P., Soldatov, N. M., Romanin, C. and Schmidt, T. (2001). Single-Molecule Imaging of L-Type Ca2+ Channels in Live Cells. Biophysical J. 81, 2639-2646.

Harms, G. S., Cognet, L., Lommerse, P. H. M., Blab, G.A. and Schmidt, T. (2001). Autofluorescent Proteins in Single-Molecule Research: Applications to Live Cell Imaging Microscopy. Biophysical J. 80, 2396-2408

Jacquier, V., Prummer, M., Segura, J.-M., Pick, H. and Vogel, H. (2006). Visualizing odorant receptor trafficking in living cells down to the single-molecule level. Proc Natl Acad Sci U S A. 103, 14325-12330.

Kasai, R. S. and Kusumi, A. (2014). Single-molecule imaging revealed dynamic GPCR dimerization. Curr Opin Cell Biol. 27, 78-86.

Kim, R. H., Li, B.D. and Chu, Q.D. (2011). The role of chemokine receptor CXCR4 in the biologic behavior of human soft tissue sarcoma. Sarcoma. 2011, 593708.

Kirchhausen, T. (2009). Imaging endocytic clathrin structures in living cells. Trends Cell Biol. 19, 596-605.

Kleemann, P., Papa, D., Vigil-Cruz, S. and Seifert, R. (2008). Functional reconstitution of the human chemokine receptor CXCR4 with G(i)/G (o)-proteins in Sf9 insect cells. Naunyn Schmiedebergs Arch Pharmacol. 378, 261-274.

Kovar, H. (2014). Blocking the road, stopping the engine or killing the driver? Advances in targeting EWS/FLI-1 fusion in Ewing sarcoma as novel therapy. Expert Opin Ther Targets. 18, 1315-1328.

Levoye, A., Balabanian, K., Baleux, F., Bachelerie, F. and Lagane, B. (2009). CXCR7 heterodimerizes with CXCR4 and regulates CXCL12-mediated G protein signaling. Blood. 113, 6085-6093.

Lill, Y., Martinez, K. L., Lill, M. A., Meyer, B. H., Vogel, H. and

Hecht, B. (2005). Kinetics of the initial steps of G protein-coupled receptor-mediated cellular signaling revealed by single-molecule imaging. Chemphyschem. 6, 1633-1640.

Luker, K. E., Gupta, M. and Luker, G. D. (2009). Imaging chemokine receptor dimerization with firefly luciferase complementation. FASEB J. 23, 823-834.

Luo, C., Pan, H., Mines, M., Watson, K., Zhang, J. and Fan, G. H. (2006). CXCL12 induces tyrosine phosphorylation of cortactin, which plays a role in CXC chemokine receptor 4-mediated extracellular signal-regulated kinase activation and chemotaxis. J Biol Chem. 281, 30081-30093.

Mangmool, S. and Kurose, H. (2011). G(i/o) protein-dependent and -independent actions of Pertussis Toxin (PTX). Toxins (Basel). 3, 884-899.

Martinez-Ramirez, A., Rodriguez-Perales, S., Melendez, B., Martinez-Delgado, B., Urioste, M., Cigudosa, J. C. and Benitez, J. (2003). Characterization of the A673 cell line (Ewing tumor) by molecular cytogenetic techniques. Cancer Genet Cytogenet. 141, 138-142.

Martins, A. S., Ordonez, J. L., Amaral, A. T., Prins, F., Floris, G., Debiec-Rychter, M., Hogendoorn, P. C. and de Alava, E. (2011). IGF1R signaling in Ewing sarcoma is shaped by clathrin-/caveolin-dependent endocytosis. PLoS One. 6, e19846.

Massotte, D. (2003). G protein-coupled receptor overexpression with baculovirus-insect cell system: a tool for structural and functional studies. Biochem Biophys Acta. 1610, 77-89.

McMahon, H. T. and Boucrot, E. (2011). Molecular mechanism and physiological functions of clathrin-mediated endocytosis. Nat Rev Mol Cell Biol. 12, 517-533.

Meckel, T., Semrau, S., Schaaf, M. J. M. and Schmidt, T. (2011). Robust assessment of protein complex formation in vivo via single-molecule intensity distributions of autofluorescent proteins. J Biomed Opt. 16, 076016

Moss, J., Bruni, P., Hsia, J. A., Tsai, S. C., Watkins, P. A., Halpern, J. L., Burns, D. L., Kanaho, Y., Chang, P. P. and Hewlett, E. L. (1984). Pertussis toxin-catalyzed ADP-ribosylation: effects on the coupling of inhibitory receptors to the adenylate cyclase system. J Recept Res. 4, 459-474.

Mueller W, Schutz D, Nagel F, Schulz S and Stumm R. (2013). Hi-

erarchical organization of multi-site phosphorylation at the CXCR4 C terminus. PLoS One. 8, e64975.

Naumann, U., Cameroni, E., Pruenster, M., Mahabaleshwar, H., Raz, E., Zerwes, H. G., Rot, A. and Thelen, M. (2010). CXCR7 functions as a scavenger for CXCL12 and CXCL11. PLoS One. 5, e9175.

Otsuka, S. and Bebb, G. (2008). The CXCR4/SDF-1 chemokine receptor axis: a new target therapeutic for non-small cell lung cancer. J Thorac Oncol. 3, 1379-1383.

Pelkmans, L. and Helenius, A. (2002). Endocytosis via caveolae. Traffic. 3, 311-320.

Papadopoulou, N., Papakonstanti, E. A., Kallergi, G., Alevizopoulos, K. and Stournaras, C. (2009). Membrane Androgen Receptor Activation in Prostate and Breast Tumor Cells: Molecular Signaling and Clinical Impact. IUBMB Life 61, 56-61.

Rey, M., Valenzuela-Fernandez, A., Urzainqui, A., Yanez-Mo, M., Perez-Martinez, M., Penela, P., Mayor, F. Jr. and SÃ¡nchez-Madrid, F. (2007). Myosin IIA is involved in the endocytosis of CXCR4 induced by SDF-1alpha. J Cell Sci. 120, 1126-1133.

Ritter, S. L. and Hall, R.A. (2009). Fine-tuning of GPCR activity by receptor-interacting protein. Nature Reviews Molecular Cell Biology 10: 819-830.

Rubin, J. B. (2009). Chemokine signaling in cancer: one hump or two? Semin Cancer Biol. 19, 116-122.

Sainz-Jaspeado, M., Lagares-Tena, L., Lasheras, J., Navid, F., Rodriguez-Galindo, C., Mateo-Lozano, S., Notario, V., Sanjuan, X., Garcia Del Muro, X., Fabra, A. and Tirado, O. M. (2010). Caveolin-1 modulates the ability of Ewing's sarcoma to metastasize. Mol Cancer Res. 8, 1489-1500.

Sainz-Jaspeado, M., Huertas-Martinez, J., Lagares-Tena, L., Martin Liberal, J., Mateo-Lozano, S., de Alava, E., de Torres, C., Mora, J., Del Muro, X. G. and Tirado, O. M. (2013). EphA2-induced angiogenesis in ewing sarcoma cells works through bFGF production and is dependent on caveolin-1. PLoS One. 8, e71449.

Samaj, J., Baluska, F., Voigt, B., Schlicht, M., Volkmann, D. and Menzel, D. (2004). Endocytosis, actin cytoskeleton, and signaling. Plant Physiol. 135, 1150-1161.

Saxton, M. J. (1993). Lateral diffusion in an archipelago Single-particle diffusion. Biophys J. 64, 1766-1780.

Schmidt, T., Schutz, G. J., Baumgartner, W., Gruber, H. J. and Schindler, H. (1996). Imaging of single molecule diffusion. Proc Natl Acad Sci U S A. 93, 2926-2929.

Schwartz, V., Kruttgen, A., Weis, J., Weber, C., Ostendorf, T., Lue, H. and Bernhagen, J. (2012). Role for CD74 and CXCR4 in clathrin-dependent endocytosis of the cytokine MIF. Eur J Cell Biol. 91, 435-449.

Semrau, S. and Schmidt, T. (2007). Particle image correlation spectroscopy (PICS): retrieving nanometer-scale correlations from high-density single-molecule position data. Biophys J. 92, 613-621.

Serge A., de Keijzer, S., Van Hemert, F., Hickman, M. R., Hereld, D., Spaink, H. P., Schmidt, T. and Snaar-Jagalska, B. E. (2011). Quantification of GPCR internalization by single-molecule microscopy in living cells. Integr. Biol. 3, 675-683.

Springael, J. Y., Urizar, E. and Parmentier, M. (2005). Dimerization of chemokine receptors and its functional consequences. Cytokine Growth Factor Rev. 16: 611-623.

Stuart, A. D. and Brown, T. D. (2006). Entry of feline calicivirus is dependent on clathrin-mediated endocytosis and acidification in endosomes. J Virol. 80, 7500-7509.

Teicher, B. A. and Fricker, S. P. (2010). CXCL12 (SDF-1)/CXCR4 pathway in cancer. Clin Cancer Res. 16, 2927-2931.

Tirado, O. M., Mateo-Lozano, S., Villar, J., Dettin, L. E., Llort, A., Gallego, S., Ban, J., Kovar, H. and Notario, V. (2006). Caveolin-1 (CAV1) is a target of EWS/FLI-1 and a key determinant of the oncogenic phenotype and tumorigenicity of Ewing's sarcoma cells. Cancer Res. 66, 9937-9947.

Tsao, P., Cao, T. and von Zastrow, M. (2001). Role of endocytosis in mediating downregulation of G-protein-coupled receptors. Trends Pharmacol Sci. 22, 91-96.

Ueda, M., Sako, Y., Tanaka, T., Devreotes, P. and Yanagida, T. (2001). Single-molecule analysis of chemotactic signaling in Dictyostelium cells. Science 294, 864-867.

van Hemert, F., Lazova, M. D., Snaar-Jagaska, B. E. and Schmidt, T. (2010). Mobility of G proteins is heterogeneous and polarized during chemotaxis. J Cell Sci. 123, 2922-2930.

Vassilieva, E. V. and Nusrat, A. (2008). Vesicular trafficking: molecular tools and targets. Methods Mol Biol. 440, 3-14.

Venkatesan, S., Rose, J. J., Lodge, R., Murphy, P. M. and Foley, J. F.

(2003). Distinct mechanisms of agonist-induced endocytosis for human chemokine receptors CCR5 and CXCR4. Mol Biol Cell. 14, 3305-3324.

Vercauteren, D., Vandenbroucke, R. E., Jones, A. T., Rejman, J., Demeester, J., De Smedt, S. C., Sanders, N. N. and Braeckmans, K. (2010). The use of inhibitors to study endocytic pathways of gene carriers: optimization and Pitfalls. Molecular Therapy. 18, 561-569.

Vila-Coro, A. J., Rodriguez-Frade, J. M., Martin De Ana, A., Moreno-Ortiz, M. C., Martinez-A, C. and Mellado, M. (1999). The chemokine SDF-1alpha triggers CXCR4 receptor dimerization and activates the JAK/STAT pathway. FASEB J. 13, 1699-1710.

Wang, L. H., Rothberg, K. G. and Anderson, R. G. (1993). Misassembly of clathrin lattices on endosomes reveals a regulatory switch for coated pit formation. J Cell Biol. 123, 1107-1117.

Wu, B., Chien, E. Y., Mol, C. D., Fenalti, G., Liu, W., Katritch, V., Abagyan, R., Brooun, A., Wells, P., Bi, F. C., Hamel, D. J., Kuhn, P., Handel, T. M., Cherezov, V. and Stevens, R. C. (2010). Structures of the CXCR4 chemokine GPCR with small-molecule and cyclic peptide antagonists. Science. 330, 1066-1071.

Yarar, D., Waterman-Storer, C. M. and Schmid, S. L. (2005). A dynamic actin cytoskeleton functions at multiple stages of clathrin-mediated endocytosis. Mol Biol Cell. 16, 964-975.

Ye, F., Breslow, D. K., Koslover, E. F., Spakowitz, A. J., Nelson, W. J. and Nachury, M. V. (2013). Single molecule imaging reveals a major role for diffusion in the exploration of ciliary space by signaling receptors. eLife 2, e00654.